Journal of The Electrochemical Society, **147** (2) 395-398 (2000)
S0013-4651(99)02-024-8 CCC: $7.00 © The Electrochemical Society, Inc.

Structural Investigations of $Li_{1.5+x}Na_{0.5}MnO_{2.85}I_{0.12}$ Electrodes by Mn X-Ray Absorption Near Edge Spectroscopy

Craig R. Horne,[a,b,g,*,z] Uwe Bergmann,[c] Jaekook Kim,[d,] Kathryn A. Striebel,[a,*] Arumugam Manthiram,[d,*] Stephen P. Cramer,[c,e] and Elton J. Cairns[a,f,***]**

[a]*Environmental Energy Technologies Division, Ernest Orlando Lawrence Berkeley National Laboratory, California, USA*
[b]*Department of Materials Science and Mineral Engineering, University of California, Berkeley, California, USA*
[c]*Structural Biology Division, Ernest Orlando Lawrence Berkeley National Laboratory, California, USA*
[d]*Texas Materials Institute, The University of Texas at Austin, Austin, Texas 78712, USA*
[e]*Department of Applied Science, University of California, Davis, California, USA*
[f]*Department of Chemical Engineering, University of California, Berkeley, California, USA*

Mn K-edge X-ray absorption near edge spectroscopy (XANES) has been performed on an amorphous, Mn-based oxide, $Li_{1.5}Na_{0.5}MnO_{2.85}I_{0.12}$, and on electrodes containing this material to determine the changes that occur in the local atomic and electronic structure with state of charge and with cycling. Comparison of the XANES data with those from λ-MnO_2, $LiMn_2O_4$, and $Li_2Mn_2O_4$ reveals that the Mn are octahedrally coordinated and reduced from Mn^{4+} to Mn^{3+} during discharge to 2 V. Additionally, it was found that the amorphous nature of $Li_{1.5}Na_{0.5}MnO_{2.85}I_{0.12}$ results in less dramatic changes upon inserting Li^+, leading to increased cycling stability and the potential for better rate capabilities within the 4-2 V range in comparison to $LiMn_2O_4$.

Manuscript submitted February 4, 1999; revised manuscript received September 26, 1999.

Li rechargeable batteries are foreseen as the means to meet the growing demand for lightweight, portable power sources. The spinel $LiMn_2O_4$ is a candidate for the positive electrode active material within Li rechargeable batteries due to a combination of low cost, benign environmental impact, and high specific energy. Unfortunately, capacity fading with cycling has hampered replacement of the currently commercialized, but higher cost and more toxic, $LiCoO_2$-based positive electrode active materials with $LiMn_2O_4$-based materials. Capacity fading in $LiMn_2O_4$ has been attributed to four main mechanisms

1. Structural breakdown due to formation of two cubic phases when $x < 0.5$ in $Li_xMn_2O_4$.[1,2]
2. Loss of active material due to dissolution of Mn^{2+} into the electrolyte at high potentials (>4 V).[3-5]
3. Decomposition of the organic electrolyte at high potentials.[6]
4. Particle fracture leading to electrically-isolated dead zone upon formation of tetragonal spinel (t-$Li_xMn_2O_4$) when $x > 1$.[5,7]

The fourth mechanism originates from the large (~6%) volume difference between coexisting cubic and tetragonal phases during the first-order phase transformation. The severity of this transformation limits the utilization of $Li_xMn_2O_4$ to $x < 1$, which corresponds to only 50% of the available capacity. This range of x is only accessible at potentials greater than 4 V, which initiates mechanisms 2 and 3, and imparts more stringent requirements for polymer electrolytes. Moreover, even if the discharge cutoff voltage upon cycling is kept above the equilibrium potential for t-$Li_xMn_2O_4$, this phase can form due to the nonequilibrium conditions of cell cycling.[8] This assertion is consistent with recent X-ray diffraction (XRD) and transmission electron microscope (TEM) studies[9-11] of cycled of $LiMn_2O_4$-based electrodes. Therefore, an electrode material that does not transform, upon changing Li^+ content, to any phase possessing a markedly different molar volume would be desirable as it would eliminate proposed capacity fade mechanisms 1 and 4 while imparting increased robustness toward overdischarge.

The mechanism for the cubic-to-tetragonal transformation has been attributed to the ferrodistortive, cooperative Jahn-Teller effect (CJTE).[1,7,12,13] This phase transformation was found to occur almost immediately upon inserting Li^+ into $LiMn_2O_4$.[7] The CJTE is cited as the driving force for the transformation because once lithiation proceeds to the concentration of Mn^{3+} (possessing four d electrons making it a Jahn-Teller ion in the high-spin state[14]) exceeds that of Mn^{4+} (possessing three d electrons making it a non-Jahn-Teller ion.[14] The electronic nature of the Jahn-Teller effect (JTE) and the necessity of an electron to compensate Li^+ insertion makes knowledge of the electronic as well as atomic structure imperative to understanding the Li^+ insertion mechanism. Such knowledge should also improve the ability to design more commercially viable electrode materials.

Recently, an alternate Mn-based oxide, $Li_{1.5}Na_{0.5}MnO_{2.85}I_{0.12}$, has shown promise as a positive electrode active material.[15,16] This material possesses high reversible capacity along with excellent cycling stability within a 4-2 V range making it suitable for use with liquid or polymer electrolytes. Additionally, the lower potential range of lithiation could avoid proposed capacity loss mechanisms 2 and 3. The amorphous nature of this material results from the low synthesis temperature and consequently prohibits structural study and the study of lithium insertion mechanisms by conventional diffraction methods. Additionally, this material is not amenable to conductivity and Seebeck coefficient measurement as the necessary monoliths or films would require high temperature densification that would most likely alter the structure.

X-ray absorption near edge spectroscopy (XANES) is an element-specific technique sensitive to the local atomic and electronic structure of the element of interest.[17] XANES studies have revealed details about the local coordination, site symmetry, oxidation state, and bond character in Mn oxides as well as Mn-containing molecular compounds.[18-21] Therefore, in order to study the atomic and electronic structure of this material and understand changes occurring upon Li^+ insertion and cycling, we performed Mn XANES on the base material and electrodes extracted from cycled cells. In this paper, we report the results of our work on $Li_{1.5}Na_{0.5}Mn_{2.85}I_{0.12}$ and compare the Li^+ insertion reaction mechanism of this material with that of $LiMn_2O_4$.

Experimental

The $Li_{1.5}Na_{0.5}MnO_{2.85}I_{0.12}$ powder used in this study was synthesized according to the procedure described by Kim and Manthiram.[15] In addition to the powder, two electrodes were studied. Electrodes and cells were fabricated as described by Kim and Manthiram.[15,16] The electrodes were extracted from coin cells cycled 40 times at a constant current density of 0.5 mA/cm² between the limits of 4 and

* Electrochemical Society Active Member.
** Electrochemical Society Student Member.
*** Electrochemical Society Fellow.
g Present address: NanoGram Corporation, Fremont, CA 94538, USA.
z E-mail: craigh@nanogram.com

S0013-4651(99)02-024-8 CCC: $7.00 © The Electrochemical Society, Inc.

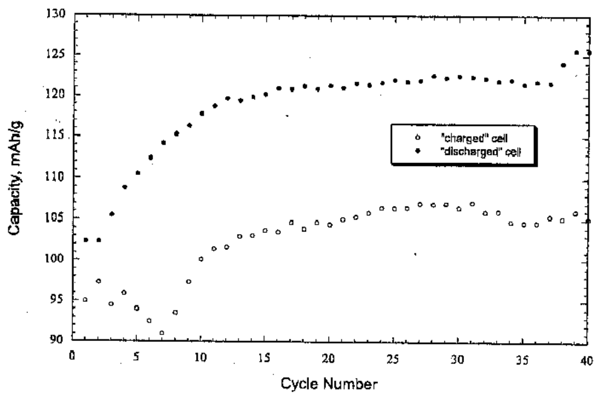

Figure 1. Discharge capacity for the two cells examined in this study. The "charged" cell denotes completion of cycling after the 41st charge and the "discharged" cell denotes completion of cycling after the 40th discharge.

2 V; the open-circuit voltage (OCV) of a fresh cell is 3.6 V. One electrode was extracted from a cycled cell after the 41st charge whereas the other came from a cycled cell after the 40th discharge. Throughout the text, the former is designated the cycled, charged electrode whereas the latter is the cycled, discharged electrode. The discharge capacities as a function of cycle number for the two cells are shown in Fig. 1. The 10-20% increase in capacity with cycling for both cells is attributed to increased electrochemical access to active material as cycling proceeded. The final composition of the cycled, charged electrode is estimated to be $Li_{1.39}Na_{0.5}MnO_{2.85}I_{0.12}$ in contrast to $Li_{2.04}Na_{0.5}MnO_{2.85}I_{0.12}$ for the cycled, discharged electrode.

The $LiMn_2O_4$ powder used was a gift from Chemetal, Inc. This powder was used to synthesize the chemically delithiated derivative, λ-MnO_2, and the chemically lithiated derivative $Li_2Mn_2O_4$. Preparation of these derivatives and verification of sample integrity was carried out as described in Ref. 22. Synthesis and verification of $ZnMn_2O_4$ was also previously described in Ref. 22.

Preparation of ($Li_{1.5}Na_{0.5}MnO_{2.85}I_{0.12}$-containing) electrode XANES samples was carried out in an Ar-filled glove bag. After extracting the electrodes, the titanium mesh was removed and the powder/C/PTFE cathode was diced and mixed in a 1:16 w/w ratio with anhydrous boron nitride (BN) using a mortar and pestle. All other samples in this study were prepared at a similar dilution; the air-sensitive $Li_2Mn_2O_4$ XANES sample was also prepared inside the glove bag. Once the powders or electrodes were well mixed with BN, approximately 0.150 g of mix were placed in a 0.17 cm thick sample holder (1.3 cm diam) and enclosed with 0.002 in. thick Kapton tape. The sample thicknesses were later determined to be approximately one absorption length at the Mn K-edge. Manganese K-edge XANES were collected at the Stanford Synchrotron Radiation Laboratory (SSRL) on bending magnet beamline 2-3 with a Si(220) double-crystal monochromator and 0.5 mm vertical, 2 mm horizontal exit slits. To avoid higher harmonics, the incident beam was detuned to 33% of maximum intensity. The ring energy was 3.0 GeV with 100 mA current at the top of the fill. Data were collected with a 0.2 eV step size through the edge region. Data reduction was performed using the EXAFSPAK analysis package available from SSRL. Transmission data from two scans of each sample were averaged and the background was subtracted using a straight line from 6310 to 6520 eV. The XANES were normalized at 6575 eV to a quartic spline fit through the background. Second derivatives were calculated after smoothing with a third order polynomial over a 1.5 eV window.

Results and Discussion

The XANES of all three $Li_{1.5}Na_{0.5}MnO_{2.85}I_{0.12}$-based samples are shown in Fig. 2, left, and the XANES from $LiMn_2O_4$, λ-MnO_2, and $Li_2Mn_2O_4$ are shown in Fig. 2, right. To facilitate comparison, the pre-edge region for each of the respective spectra are magnified

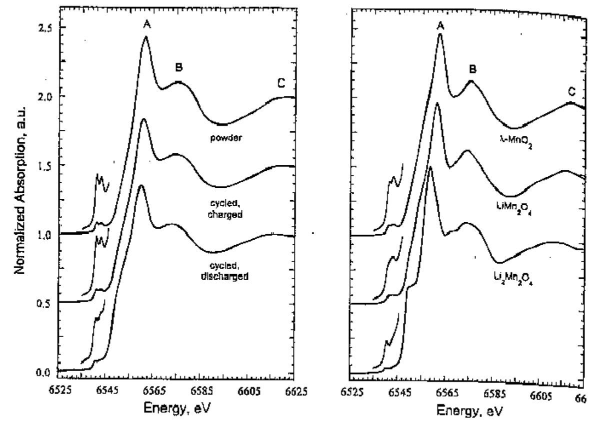

Figure 2. Mn K-edge XANES from: (left) $Li_{1.5}Na_{0.5}MnO_{2.85}I_{0.12}$ (powder, cycled, charged electrode, and cycled discharged electrode, and (righ $LiMn_2O_4$ and its chemically delithiated (λ-MnO_2) and lithiated (Li_2Mn_2O derivatives.

by a factor of 5 in Fig. 2 left and right. Table I contains the energ position of salient features within the XANES. Maxima A, B, and C as defined in Fig. 2 left and right, were identified with EXAFSPAK Positions of other spectral features denoted in Table I with Greek letters were identified from the XANES second derivatives, shown i Fig. 3 left and right, for each of the respective spectra. For clarity, smaller energy range is used for the XANES second derivative tha for the XANES shown in Fig. 2. The features identified as α, β, γ ϵ, and η were obtained from local minima whereas feature δ locate the point at which the second derivative is zero as discussed below.

First, we compare the XANES of the $Li_{1.5}Na_{0.5}MnO_{2.85}I_{0.1}$ powder with that of the delithiated spinel, λ-MnO_2 $Li_{1.5}Na_{0.5}MnO_{2.85}I_{0.12}$ possesses an average Mn oxidation state clos to +4,[15] approximately the same as that of λ-MnO_2 (the lattice para meter of which corresponds to that reported in the literature fo $Li_{0.2}Mn_2O_4$ [22]). To begin with, the $Li_{1.5}Na_{0.5}MnO_{2.85}I_{0.12}$ powde XANES reveals that the Mn are octahedrally coordinated, presumably by oxygen as at least a portion of the iodine is tied up in crystalline $NaIO_3$.[23] This is concluded from the shape of the edge and it similarity, in particular the pre-edge region, to that of λ-MnO_2. The pre-edge region is assigned to 1s → 3d transitions, and weak intensity in this region is indicative of octahedral coordination as opposed to tetrahedral coordination from which strong pre-edge intensity is found.[19,21] The energy positions of the spectral features shown in Table I compare well with those of λ-MnO_2 except for that of the main edge (feature A). The slightly lower main peak energy in the $Li_{1.5}Na_{0.5}MnO_{2.85}I_{0.12}$ powder could be due to the slightly lower Mn oxidation state, a larger Mn–O bond length, and/or a more covalent Mn–O bond. Any of these characteristics, singly or in combination, will lessen the 2s core-hole binding energy leading to a lower main peak energy. However, concomitant lower energy positions of other features would also be expected, and so, we cannot ascribe the source for lower main peak position in $Li_{1.5}Na_{0.5}MnO_{2.85}I_{0.12}$ at this time.

It should be noted that a recent paper by Liu *et al.*[24] concluded that the average Mn oxidation state in $LiMn_2O_4$ was approximately +4 using a combination of Mn $L_{II,III}$-edge and Mn K-edge XANES. This assertion runs counter to recent reports that $LiMn_2O_4$ is a mixed Mn^{3+}/Mn^{4+} oxide through measurement of the Mn K-edge XANES,[25,26] Mn 2p X-ray photoelectron spectroscopy,[27] and magnetic properties.[28] Additionally, the presence of Mn^{3+} is required for the CJTE to take place as described in the first section of this paper. Liu *et al.* arrived at their conclusion by comparing the edge positions of the main L_{III} feature of the Mn $L_{II,III}$ spectra and what is called feature α in this study of the Mn K spectra to those from MnO_2 and Mn_2O_3. We find similar agreement between the positions of feature α for $LiMn_2O_4$ and λ-MnO_2 along with $Li_{1.5}Na_{0.5}MnO_{2.85}I_{0.12}$ but

Journal of The Electrochemical Society, 147 (2) 395-398 (2000)
S0013-4651(99)02-024-8 CCC: $7.00 © The Electrochemical Society, Inc.

Table I. Positions for XANES spectral features noted in Fig. 2, 3, and 4. Positions of the features denoted by Greek letters were determined from the second derivatives (Fig. 3) while the other peak positions were found using EXAFSPAK.

Sample	Energy position, eV								
	α	β	γ	δ	ϵ	A	η	B	C
powder	6541.1	6543.4	6550.8	—	6553.8	6561.4	—	6575.4	6620.6
cycled-charged	6541.1	6543.4	6550.4	—	6553.8	6560.9	—	6574.9	6619.6
cycled-discharged	6540.8	6543.1	6549.7	—	6552.8	6560.2	—	6573.2	6616.4
λ-MnO_2	6541.1	6543.2	6550.3	—	6555.4	6562.1	—	6575.4	6619.5
$LiMn_2O_4$	6541.1	6542.9	6549.6	—	6553.5	6561.1	—	6573.9	6616.5
$Li_2Mn_2O_4$	6540.6	—	6549.1	6550.8	—	6558.3	6567.0	6573.6	6613.5
$ZnMn_2O_4$	6540.4	—	6551.7	6553.3	—	6560.0	—	6572.0	6612.4

the main peak energy shifts are different (see Table I). A recent ^7Li NMR and magnetic susceptibility study has shown that the relative degree of covalency within $LiMn_2O_4$ increases markedly upon delithiating $LiMn_2O_4$ to form λ-MnO_2.[29] This agrees well with $X\alpha$ calculations of $[MnO_6]$ octahedra showing that the degree of covalency is larger for $[Mn^{4+}O_6]$ octahedra compared to $[Mn^{3+}O_6]$ octahedra.[30] The covalency increase induced by oxidizing a mixed Mn^{3+}/Mn^{4+} oxide, such as $LiMn_2O_4$, into 100% Mn^{4+} can counter to some degree the chemical shift expected based upon the completely ionic picture presented by Liu *et al.*[24]

A final observation is that the rising edge for the $Li_{1.5}Na_{0.5}MnO_{2.85}I_{0.12}$ powder is smoother than that of λ-MnO_2. Inflections in the edge similar to those found in the λ-MnO_2 XANES were shown to originate from increased distortion of octahedral bond angles from 90° within the $[CuO_6]$ octahedra of copper oxides[31,32] and more recently within the $[MnO_6]$ octahedra of manganese oxides.[21] Structural refinements have consistently shown, through an increase of the spinel *u* parameter, that the octahedral bond angles are more distorted in delithiated $LiMn_2O_4$ as compared to the parent materials.[1,2,33] The relatively, smooth rising edge of the $Li_{1.5}Na_{0.5}MnO_{2.85}I_{0.12}$ XANES, therefore, suggests that the $[MnO_6]$ octahedral bond angles are less distorted than those for λ-MnO_2 or $LiMn_2O_4$.

Next, the effects of lithiating $Li_{1.5}Na_{0.5}MnO_{2.85}I_{0.12}$ are discussed. As is the case with the spinel system, the data in Table I show that upon discharging, the edge moves to lower energy. This is consistent with reduction of the Mn^{4+} in $Li_{1.5}Na_{0.5}MnO_{2.85}I_{0.12}$ by the electron-compensating insertion of a Li^+ as also is found to occur in the spinel system.[13,22] The inflection in the edge of the cycled, discharged electrode XANES implies that the octahedra become distorted during lithiation. The similarity of the pre-edge region with that of the $Li_2Mn_2O_4$ XANES makes this conclusion firmer. This point is discussed in more detail below. The data of Fig. 2 left and 3 left show that the powder and cycled, charged electrode possess comparable characteristics, aside from the growth of feature γ, suggesting that the local structure is not grossly altered by repeated cycling. This is particularly evidenced by the pre-edge regions. Thus the distortion observed upon lithiating $Li_{1.5}Na_{0.5}MnO_{2.85}I_{0.12}$ is not as destructive, compared to the spinel system, to the structural integrity. However, the lower energy of several features within the cycled, charged electrode XANES as compared to the powder could signify that some areas of reduced (lithiated) material remain.

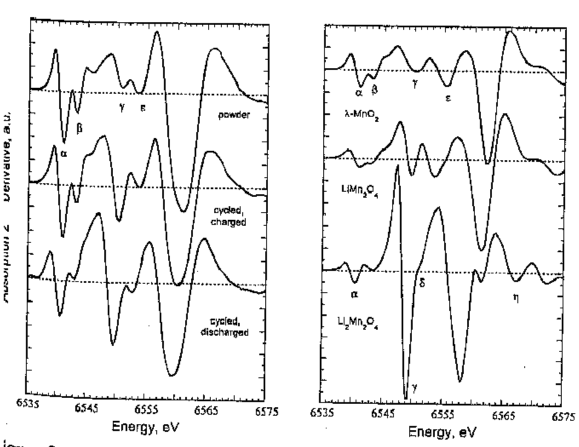

igure 3. Comparison of Mn K-edge XANES second-derivatives from (left) $_{1.5}Na_{0.5}MnO_{2.85}I_{0.12}$ (powder), cycled, charged electrode, and cycled discharged electrode, and (right) $LiMn_2O_4$ and its chemically delithiated (λ-MnO_2) and lithiated ($Li_2Mn_2O_4$) derivatives.

To further elucidate our assertion that there is a distortion of $[MnO_6]$ octahedra upon lithiating $Li_{1.5}Na_{0.5}MnO_{2.85}I_{0.12}$ we compare the XANES of the cycled, discharged electrode with those from $Li_2Mn_2O_4$ and the tetragonal, Mn^{3+} spinel, $ZnMn_2O_4$. $ZnMn_2O_4$ belongs to the same space group as $Li_2Mn_2O_4$ and possesses approximately the same distortion parameter (*c*/*a* ratio), 1.15 [34] *vs.* 1.18.[1,13,25,35] The nearly identical pre-edge shapes of the three XANES in Fig. 4 indicates that all are tetragonally distorted whereas the lack of feature δ in the cycled, discharged XANES implies that the distortion parameter of the cycled, discharged electrode is not as large as that for either tetragonal spinel. The similar main peak positions of the cycled, discharged electrode and $ZnMn_2O_4$ lead to the conclusion that upon lithiating $Li_{1.5}Na_{0.5}MnO_{2.85}I_{0.12}$ the Mn^{4+} are reduced to Mn^{3+}. This in turn would be the source of the distorted structure within lithiated $Li_{1.5}Na_{0.5}MnO_{2.85}I_{0.12}$ because according to the Jahn-Teller theory,[36,37] the degenerate E_g ground-state of an octahedrally coordinated, localized Mn^{3+} is unstable with respect to a tetragonal distortion. Finally, the differences of the edge shapes between the discharged, cycled electrode and $Li_2Mn_2O_4$ XANES merits discussion. The distinct edge step and a satellite peak above the main peak (denoted by feature η in the second derivative of Fig. 4 right) are associated with the Li^+ inserted into the interstitial octahedral sites of the spinel as they are absent in the XANES of $ZnMn_2O_4$, and other tetragonal Mn(III) spinels.[22] We have asserted that these features found within the $Li_2Mn_2O_4$ XANES are indicative of an increased degree of covalency.[22] An increased degree of covalent character within the Li–O bond upon lithiating $LiMn_2O_4$ would be a source of the more sluggish insertion reaction kinetics observed in the 3 V region of the spinel with respect to the 4 V region.[12,38,39] Therefore, the difference observed in the XANES indicates that $Li_{1.5}Na_{0.5}MnO_{2.85}I_{0.12}$ should possess faster Li^+ transport at low voltages.

Conclusions

Our XANES study of $Li_{1.5}Na_{0.5}MnO_{2.85}I_{0.12}$ along with electrodes containing this material extracted from discharged and cycled cells has revealed important information concerning the electronic and atomic structure of this material and its Li^+ insertion reaction mechanism. The data reveals that the Mn sites in the $Li_{1.5}Na_{0.5}MnO_{2.85}I_{0.12}$ powder are primarily $[Mn^{4+}O_6]$ octahedra. Upon lithiation (discharging), the Mn^{4+} are reduced to Mn^{3+} which results in a tetragonal distortion of the $[MnO_6]$ octahedra due to the JTE. This distortion is reversible

S0013-4651(99)02-024-8 CCC: $7.00 © The Electrochemical Society, Inc.

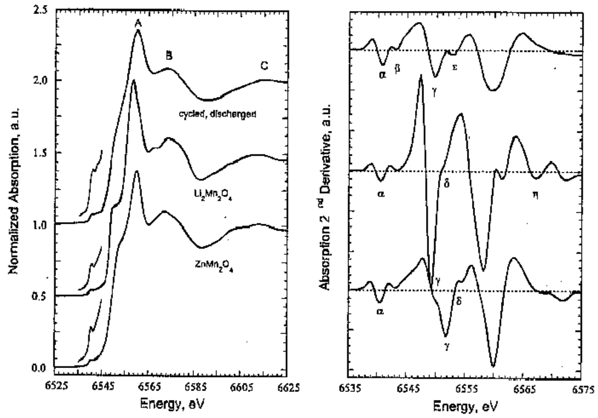

Figure 4. Comparison of (left) Mn K-edge XANES and (right) XANES second derivatives from the cycled discharged electrode and the tetragonal spinels $Li_2Mn_2O_4$ and $ZnMn_2O_4$.

upon delithiation (charging); the reversibility does not appear to be affected by cycling. The spectroscopic results do not indicate that reduction of Mn^{3+} to Mn^{2+} occurs when discharging this material down to 2 V.

Comparing and contrasting this Li^+ insertion mechanism with that occurring in the $LiMn_2O_4$ system showed that the Li^+ can be accommodated in the amorphous $Li_{1.5}Na_{0.5}MnO_{2.85}I_{0.12}$ with a much less severe effect on atomic and electronic structure. The XANES provide evidence that the distortion parameter of lithiated $Li_{1.5}Na_{0.5}MnO_{2.85}I_{0.12}$ is less than that of $Li_2Mn_2O_4$ and $ZnMn_2O_4$ whereas the amorphous nature of $Li_{1.5}Na_{0.5}MnO_{2.85}I_{0.12}$ provides the open space to accommodate the JTE distortion in a noncooperative manner. The absence of the distinct edge step and satellite peak in the cycled, discharged electrode XANES indicates that the electronic structure of $Li_{1.5}Na_{0.5}MnO_{2.85}I_{0.12}$ is not as greatly perturbed by lithiation when compared to $LiMn_2O_4$. These findings indicate that the lower degree of atomic and electronic structural change upon altering the Li^+ content of $Li_{1.5}Na_{0.5}MnO_{2.85}I_{0.12}$, with respect to $LiMn_2O_4$, within the 4-2 V range provides increased cycling stability. Furthermore, the absence of XANES features indicative of an increased degree of covalency upon inserting Li^+ suggests that the rate capability of $Li_{1.5}Na_{0.5}MnO_{2.85}I_{0.12}$ within this potential window should be higher in comparison to the $LiMn_2O_4$ system.

Our XANES results indicate that amorphous, Mn-based materials possess electronic and atomic structural characteristics that afford more benign accommodation of Li^+ and the compensating electron. These intrinsic traits suggest that such materials are promising candidates for use in positive electrodes to attain longer-lasting and higher-power Li rechargeable batteries.

Acknowledgments

This work was supported by the Director, Office of Energy Research, Office of Basic Energy Sciences, Chemical Sciences Division of the U.S. Department of Energy, under contract no. DE-AC03-76SF00098 to the Ernest Orlando Lawrence Berkeley National Laboratory. The Stanford Synchrotron Radiation Laboratory is funded by the Department of Energy, Basic Energy Sciences. Tl work at The University of Texas at Austin was supported by tl National Science Foundation grant DMR-9401999.

Lawrence Berkeley National Laboratory assisted in meeting the public tion costs of this article.

References

1. T. Ohzuku, M. Kitagawa, and T. Hirai, *J. Electrochem. Soc.*, **137**, 769 (1990).
2. K. Kanamura, H. Naito, T. Yao, and Z. Takehara, *J. Mater. Chem.*, **6**, 33 (1996).
3. R. J. Gummow, A. de Kock, and M. M. Thackeray, *Solid State Ionics*, **69**, : (1994).
4. D. H. Jang, Y. J. Shin, and S. M. Oh, *J. Electrochem. Soc.*, **143**, 2204 (1996).
5. S. J. Wen, T. J. Richardson, L. Ma, K. A. Striebel, P. N. Ross, and E. J. Cairn *J. Electrochem. Soc.*, **143**, L136 (1996).
6. J. M. Tarascon and D. Guyomard, *Electrochim. Acta*, **38**, 1221 (1993).
7. M. M. Thackeray, W. I. F. David, P. G. Bruce, and J. B. Goodenough, *Mater. Re Bull.*, **18**, 461 (1983).
8. M. M. Thackeray, *J. Electrochem. Soc.*, **142**, 2558 (1995).
9. Y. Bito, H. Murai, S. Ito, M. Hasegawa, and Y. A. Toyoguchi, in *Proceedings of tl Symposium on Rechargeable Lithium and Lithium-Ion Batteries*, S. Megahe B. M. Barnett, and L. Xie, Editors, PV 94-28, p. 461, The Electrochemical Socie Proceedings Series, Pennington, NJ (1995).
10. W. Liu, K. Kowal, and G. C. Farrington, *J. Electrochem. Soc.*, **143**, 3590 (1996).
11. M. M. Thackeray, Y. Shao-Horn, A. J. Kahaian, K. D. Kepler, E. Skinner, J. Vaughey, and S. A. Hackney, *Electrochem. Solid State Lett.*, **1**, 7 (1998).
12. J. B. Goodenough, M. M. Thackeray, W. I. F. David, and P. G. Bruce, *Rev. Chen Miner.*, **21**, 435 (1984).
13. E. J. Cairns, C. R. Horne, B. J. Weiss, M. M. Grush, and S. P. Cramer, in *Proceec ings of the 2nd International Symposium on New Materials for Fuel Cells an Modern Battery Systems*, Montreal, Canada, July 6-10, 1997, O. Savadogo an P. R. Roberge, Editors, École Polytechnique de Montrèal, 1997, p. 336.
14. F. A. Cotton, *Advanced Inorganic Chemistry*, 3rd ed., p. 564, John Wiley & Son New York (1972).
15. J. Kim and A. Manthiram, *Nature*, **390**, 265 (1997).
16. J. Kim and A. Manthiram, *Electrochem. Solid-State Lett.*, **2**, 55 (1999).
17. A. Bianconi, in *X-Ray Absorption: Principles, Applications, Techniques of EXAF SEXAFS, and XANES*, D. C. Koningsberger and R. Prins, Editors, p. 573, Joh Wiley & Sons, New York (1988).
18. G. L. Glen and C. G. Dodd, *J. Appl. Phys.*, **39**, 5372 (1968).
19. M. Belli, A. Scafati, A. Bianconi, S. Mobilio, L. Palladino, A. Reale, and E. Burat tini, *Solid State Commun.*, **35**, 355 (1980).
20. L. A. Grunes, *Phys. Rev. B.*, **27**, 2111 (1983).
21. A. Manceau, A. I. Gorshkov, and V. A. Drits, *Am. Mineral.*, **77**, 1133 (1992).
22. C. R. Horne, U. Bergmann, M. M. Grush, E. J. Cairns, and S. P. Cramer, *J. Phys Chem. B*, Submitted.
23. A. Manthiram, J. Kim, and S. Choi, *Mater. Res. Soc. Symp. Proc.*, In press.
24. R. S. Liu L. Y. Jang, J. M. Chen, Y. C. Tsai, Y. D. Hwang, and R. G. Liu, *J. Soli State Chem.*, **128**, 126 (1997).
25. B. Ammundsen, D. J. Jones, J. Roziére, and G. R. Burns, *Chem. Mater.*, **8**, 279 (1996).
26. Y. Shiraishi, I. Nakai, T. Tsubata, T. Himeda, and F. Nishikawa, *J. Solid State Chem.*, **133**, 587 (1997).
27. N. Treuil, C. Labrugere, M. Menetrier, J. Portier, G. Campet, A. Deshayes, J. C. Frison, S. J. Hwang, S. W. Song, and J. H. Chow, *J. Phys. Chem. B*, **103**, 210C (1999).
28. C. Masquelier, M. Tabuchi, K. Ado, R. Kanno, Y. Kobayashi, Y. Maki, O. Nakamura, and J. B. Goodenough, *J. Solid State Chem.*, **123**, 255 (1996).
29. B. Gee, C. R. Horne, E. J. Cairns, and J. A. Reimer, *J. Phys. Chem. B*, **102**, 10142 (1998).
30. D. M. Sherman, *Am. Mineral.*, **69**, 788 (1984).
31. J. Garcia, M. Benfatto, C. R. Natoli, A. Bianconi, A. Fontaine, and H. Tolentino, *Chem. Phys.*, **13**, 2295 (1989).
32. J. Garcia, A. Bianconi, M. Benfatto, and C. R. Natoli, *J. Phys.*, **47** C8-49 (1986).
33. C. Fong, B. J. Kennedy, and M. M. Elcombe, *Z. Kristallogr.*, **209**, 941 (1994).
34. N. Yanamoto, S. Kawano, N. Achiwa, and S. Higashi, *FOFUA*, **30**, 48 (1983).
35. W. I. F. David, M. M. Thackeray, L. A. De Picciotto, and J. B. Goodenough, *J. Solid State Chem.*, **67** 316 (1987).
36. H. A. Jahn and E. Teller, *Proc. R. Soc. London*, **A161**, 220 (1937).
37. H. A. Jahn, *Proc. R. Soc. London*, **A164**, 117 (1938).
38. J. Barker, R. Pynenburg, and R. Koksbang, *J. Power Sources*, **52**, 185 (1994).
39. K. S. Striebel, A. Rougier, C. R. Horne, R. P. Reade, and E. J. Cairns, *J. Electrochem. Soc.*, **146**, 4339 (1999).